

## Modelling Homogenization Heat Treatment for AA3XXX Alloys

Qiang Du<sup>1</sup>, Wareen J. Poole<sup>1</sup>, Mary A. Wells<sup>2</sup>, Nick Parson<sup>3</sup>

<sup>1</sup> Department of Materials Engineering, the University of British Columbia, 309-6350 Stores Road, Vancouver, V6T 1Z4, Canada

<sup>2</sup> Department of Mechanical and Mechatronics Engineering, University of Waterloo, 200 University Avenue West, Waterloo, N2L 3G1, Canada

<sup>3</sup> Rio Tinto Alcan, 945 Princess Street, Kingston, K7L 5T4, Canada

The evolution of microstructure during solidification and homogenization of AA3xxx alloys involves microsegregation of alloying elements, the nucleation, growth and coarsening of intra-granular dispersoids and the growth/dissolution of inter-granular constituent particles. These phenomena (except for nucleation) are controlled by the diffusion of alloying elements, which occurs either across the dendrites (~10  $\mu\text{m}$ , referred to as long-range) or around dispersoids (~0.01 to 1  $\mu\text{m}$ , referred to as short-range). In this paper, the microstructure evolution has been simulated using a comprehensive fully CALPHAD-coupled model, which consists of a nucleation model, 1D Pseudo Front Tracking (PFT) model for the long-range diffusion and a Kampmann-Wagner Numerical (KWN) model for the short-range diffusion. The simulation results have been validated using experimental measurements. Our investigation demonstrates the ability of the model to reveal the influence of the initial as-cast microstructure on the precipitation kinetics and to track the evolution of the microstructure features such as precipitate free zone (PFZ), the number density, size distribution of dispersoids and the type and fractions of constituent particles. The model output can readily be used as an input for downstream process models.

**Keywords:** AA3xxx, homogenization heat treatment, modeling, precipitation, CALPHAD

### 1. Introduction

AA3xxx alloys are manganese containing commercial aluminum alloy which have applications in many industrial sectors. Homogenization treatment is an important process in the manufacturing route. It has an important influence on the deformation, recovery and recrystallization process occurring during the subsequent thermo-mechanical processes. The evolution of microstructure during industrial homogenization treatment has been extensively studied from both experimental [1,2] and modeling perspectives [3,4,5]. The starting point for homogenization is the as-cast microstructure, which mainly consists of primary aluminum with a small amount of inter-granular second phases. The distinguishing microstructure feature for primary phases is the average secondary dendrite arm spacing, which is at the scale of several tens of microns. The secondary phase consists of rod or plate like particles hereafter referred to as constituent particles. The constituent particles have been identified as a mixture of  $\text{Al}_6(\text{Mn}, \text{Fe})$  and  $\alpha\text{-Al}(\text{Mn}, \text{Fe})\text{Si}$  with a size of ~ 1-5  $\mu\text{m}$ .

Under industrial solidification conditions severe microsegregation exists, i.e, the primary phase is super-saturated and the compositional profile across a secondary arm is non-uniform. Homogenization heat treatment transforms the as-cast microstructure closer to equilibrium through two primary precipitation mechanisms. One is the growth and transformation of constituent particles, in which the diffusion at the scale of secondary dendrite arm spacing, hereafter referred as long-range diffusion, plays a very important role. This long range diffusion transports the alloying components (Fe, Mn and Si) through the supersaturated primary phase matrix to the interdendritic region, which may cause the transformation of the constituent particles from  $\text{Al}_6(\text{Mn}, \text{Fe})$  to  $\alpha\text{-Al}(\text{Mn}, \text{Fe})\text{Si}$ . The second precipitation mechanism is the nucleation, growth and coarsening of smaller  $\alpha\text{-Al}(\text{Mn}, \text{Fe})\text{Si}$  particles, hereafter referred to as dispersoids, in the intra-granular region. This reaction leads to a reduction or elimination of the super-saturation in the primary aluminum. According to experimental studies in the literature for AA3003 alloy, these dispersoids can grow to sizes of ~200 nm and the

peak number density can reach  $1000/\mu\text{m}^3$  [1]. For these dispersoids, diffusion at the scale of several hundred nm (i.e the inter-dispersoid spacing) hereafter referred to as short-range diffusion, plays an important role during their growth and coarsening.

Clearly, the long- and short-range diffusion of solute are not separate from each other, i.e they are coupled. The growth/coarsening of inter-granular constituent particles requires the long-range transport of Fe and Mn, which are also involved in the growth/coarsening of inter-granular dispersoids. For Si, as suggested by Li and Arnberg [5], the interdendritic phase transformation from  $\text{Al}_6(\text{Fe},\text{Mn})$  to the  $\alpha\text{-Al}(\text{Mn},\text{Fe})\text{Si}$  phase requires its long-range transportation. Since the Si concentration in the solid solution has a strong influence on the equilibrium solid solution level of Mn and Fe, the diffusion of Si, influences the rate of dispersoid precipitation. During the coarsening stage, which occurs during the later stages of homogenization, the volume fraction of dispersoids tends to decrease while the fraction of constituent particles increases because the latter has the size advantage. Therefore, it is very important to have a multi-scale model which could take into account the interaction of long and short range diffusion of all alloying components.

Lok and Miroux attempted to solve this problem by developing an analytical model [4]. However their model is limited to a single diffusing component (Mn) and does not take into account the transformation kinetics from a  $\text{Al}_6(\text{Mn}, \text{Fe})$  to an  $\alpha\text{-Al}(\text{Fe},\text{Mn})\text{Si}$  constituent particle. Gandin and Jacot proposed a comprehensive model [3], which is able to capture the interaction between long and short range diffusion. They have taken into account multi-component diffusion and the transformation kinetics between  $\text{Al}_6(\text{Mn}, \text{Fe})$  and  $\alpha\text{-Al}(\text{Fe},\text{Mn})\text{Si}$  constituent particles. However they employed a solubility product method for the evaluation of the Gibbs-Thomson effect. Although the solubility product constants were computed from CALPHAD software and a commercial thermodynamic database, the solubility product method introduces a level of approximation which can be quite important in multi-component diffusion problems. This observation has motivated us to extend their approach to be fully-CALPHAD coupled. The work related to this extension will be reported in a separate paper and only a brief description is given here in the following section. The foci of this paper are the application of the extended model to homogenization heat treatment for three AA3xxx alloys and the experimental validation of the obtained simulation results.

## 2. Model Descriptions

This modeling work consists of three parts: a nucleation model, a 1D Pseudo Front Tracking (PFT) model for intergranular phase transformations and a KWN model for intragranular precipitate kinetics. The 1D PFT and KWN models are coupled with each other via the average compositional variables. In addition, these three sub-models have to be coupled with the CALPHAD software to be applicable to commercial alloys. In addition to a thermodynamic database, its input parameters include the chemistry of the alloy, the experimentally measured secondary dendrite arm spacing, the thermo-physical properties such as diffusivities and surface energy and the nucleation parameters (for example, nucleation undercooling for the formation of constituent particles, and heterogeneous nucleation sites and wetting angle for modeling heterogeneous dispersoid nucleation). With these input parameters, the model is able to simulate: 1) the micro-segregation and the formation of constituent particles during solidification, 2) the removal of the micro-segregation 3) the transformation rate of constituent particles and 4) the precipitation of intergranular dispersoids during homogenization. Its output includes: the evolution of compositional profiles of any alloying element, size distribution and number density of dispersoids, precipitate free zone (PFZ), and type and fractions of constituent particles etc, which are ready to be used in downstream process models.

### 2.1 Nucleation Model

Nucleation, being of stochastic nature, plays a very important role in precipitation kinetics but remains a challenge to model quantitatively. Models for nucleation are generally referred to as either “homogeneous” or “heterogeneous” and the later prevails under the scenarios considered in this

paper. The physical properties required to compute nucleation rate are the number of nucleation sites per unit volume, the interfacial energy, the diffusivity of an alloying component in the matrix, the driving force for precipitate per unit volume, the matrix mean solute atom fraction, the mean atomic volume within precipitates and the lattice parameter of matrix phase. Please refer to [3, 6, 7] and the references therein for more details on the nucleation model.

## 2.2 1D Pseudo Front Tracking Method

The 1D PFT model is adopted here to describe the long range diffusion. The details of this model can be found in references [8,9] and only a brief introduction is given here. The model is based on the following assumptions: (i) the composition of the intergranular region is uniform (ii) the intergranular region is locally in thermodynamic equilibrium and all phases have uniform concentrations, (iii) the long range diffusion affects the intergranular region in a uniform manner. The solution of the problem is based on a finite volume method. A volume element or cell of the mesh has three possible states: matrix, intergranular mixture, or interface. A layer of interface cells always separates the matrix and the intergranular mixture. An explicit formulation using the finite volume method provides a variation of solute concentrations in each cell with matrix states.

## 2.3 KWN model

The KWN model we employed in our simulation is a fully-CALPHAD coupled multi-component precipitation kinetics model (via a table look-up technique based on Thermocalc with the TTAL6 database). It is developed using classical nucleation, growth and coarsening theory. The model is capable of predicting the evolution of precipitate size distribution, number density, composition and fraction. It has the following features enabling its application to industrial relevant alloys:

1. It is able to utilize commercial thermodynamic databases, i.e., in this case, TTAL6 database.
2. The assumption that the precipitate phase is purely stoichiometric is not necessary. Depending on its diffusivity, the diffusion of an alloying element inside a precipitate has been modelled either as infinite diffusion or non-diffusion.
3. The numerical solution to the proposed model is based on the Predictor-Corrector methodology with an adaptive time step control. It is very efficient compared to the iteration techniques that have been traditionally used [6].

## 3. Results and Discussions

The solidification and homogenization heat treatment of an AA3003 alloy were simulated to predict the evolution of microstructure features that are vital to downstream processing such as extrusion. The input parameters to the calculation are listed in Table 1.

The first prediction is the as-cast microstructure consisting of microsegregation and the fraction of secondary phases and their type. Fig. 1 shows the calculated as-cast compositional profiles along a secondary arm (the curve with square marks). As expected, being depleted at the core of the secondary arm, the solutes become richer and richer as the interdendritic region is approached. At a distance of  $\sim 6.5 \mu\text{m}$  away from the core, the Mn level starts to decrease due to the formation of the interdendritic Mn rich constituent particles. Please note the last data point of this curve ( $\sim 8 \mu\text{m}$  away from the core) shows the Mn level in the primary phase only and does not include the contributions from the constituent particles. Of course the interdendritic region was enriched as the solidification proceeded and the simulation predicted 1.9at%  $\text{Al}_6\text{Mn}$  and 0.12at%  $\alpha\text{-Al}(\text{Mn,Fe})\text{Si}$  phase. The simulated as-cast microstructure was validated by comparing the predictions with the measured value of the average Mn solid solution solute level using Electrical Probe Micro-Analysis (EPMA) as shown in Table 2 (the as-cast column).

During the homogenization heat treatment, both i) long range diffusion which removes the spatial inhomogeneity of solutes by the growth of the constituent particles and ii) short range diffusion which controls dispersoid growth, coarsening and ultimately dissolution occurs. The diffusion on these two different length scales as well as their interaction has been well tracked by the simulation. Fig.1

shows the Mn solid solution solute level across the secondary arm at various times during the homogenization heat treatment described in Table 1.

Table 1: Input parameters for the simulation

Parameter	Value or explanations
<b>System</b>	
Chemistry	Al-0.5wt%Fe-1.25wt%Mn-0.1wt%Si
Domain Size	1DPFT model, 8.6 $\mu\text{m}$ consisting of 10 cells KWN: 0.86 $\mu\text{m}^3$
Thermal (Solidification and Homogenization treatment)	History and heat 0.1°C/s cooling from the liquid state until full solidification. 2°C/s during post-solidification cooling until 100°C. 150 °C/Hour heating to 550°C. 50°C/Hour heating to 600°C. Then isothermal holding at 600°C for up to 24 hours.
Dispersoid type	$\alpha$ -Al(Mn,Fe)Si phase
<b>Thermo-Physical properties</b>	
Molar volume	$9.0 \times 10^{-6} \text{ m}^3/\text{mol}$
Interface energy	0.15 J/m <sup>2</sup>
Diffusivity	$D_{\text{Fe}}^{\text{FCC}} = 0.362 \text{Exp}\left(-\frac{214000.0}{RT}\right)$ $D_{\text{Mn}}^{\text{FCC}} = 0.0135 \text{Exp}\left(-\frac{211500}{RT}\right)$ $D_{\text{Si}}^{\text{FCC}} = 0.0000138 \text{Exp}\left(-\frac{117600}{RT}\right)$
Gibbs-Thomson phase diagram	Calculated by Thermo-Calc with TTAL6 database, table-look-up technique is employed for the coupling with KWN model
<b>Nucleation Parameters</b>	
Nucleation temperature for constituent particles	250 °C for ALPHA and 634 °C for Al <sub>6</sub> Mn.
Heterogeneous nucleation site	$1.5 \times 10^{21} /\text{m}^3$
The wetting angle	45°

Table 2: EMPA measured and simulated average Mn composition (in wt%)

	As Cast	2.8 HT, 431 °C	3.0 HT, 462 °C	3.3 HT, 516 °C	5.0 HT, 598 °C	8.0 HT, 595 °C	28 HT, 600 °C
EPMA	1.15	1.1	1.1	1.1	0.9	0.7	0.6
Simulation	1.175	1.175	1.175	1.167	0.961	0.692	0.568

Initially the Mn solute level decreases from the as-cast level as shown by the curve with diamond markers (T=471 °C) in Fig.1. This decrease is mainly due to the nucleation and growth of a large number of Fe and Mn bearing dispersoids as shown in Fig.2 (the curve with diamond markers). Long range diffusion is insignificant at this low temperature due to the combined effects of low Mn diffusivity and the long diffusion distance (~10  $\mu\text{m}$ ). In contrast, short-range diffusion which controls the dispersoid nucleation and growth, was effective due to the small diffusion distances involved (~0.1  $\mu\text{m}$ ). The dispersoid growth altered the compositional profile and would have a direct impact on the long range diffusion process. Long range diffusion became significant when the temperature increased to 550 °C and higher. At these temperatures, the dispersoid fraction in the region adjacent to the interdendritic region underwent a rapid decrease (see the curve with the X markers in Fig.2 and compare it with the curve with the diamond markers). This occurred because Mn had been transported by the long range diffusion to the interdendritic region for the growth of constituent particles. At the start of soaking, as shown by the curve with star markers in Fig.2, a precipitation free

zone (PFZ) appeared as a result of long range diffusion. As time increases, the region influenced by the long range diffusion spreads further away from the interdendritic region and the PFZ grows. At longer times (i.e. after 3 hours of soaking), the Mn compositional profile was almost flat (circle markers in Fig.1) and PFZ advanced further to the center of the dendritic arm (see the curve with circle markers in Fig.2). After 15 hours of soaking, the Mn compositional profile was flat (+ markers in Fig.1) while there were still some dispersoids left within the center region (+ markers in Fig.2).

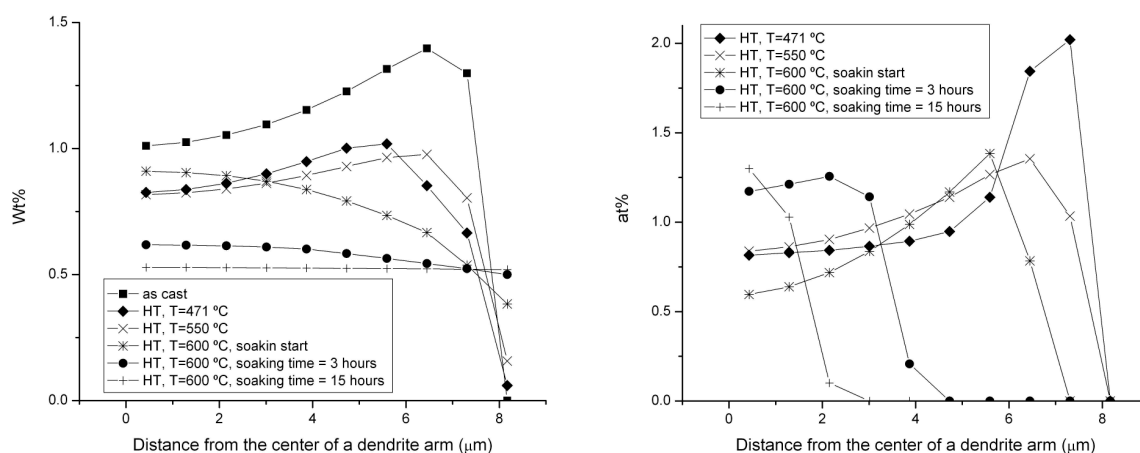


Fig. 1 The calculated Mn compositional profiles Fig.2 The calculated dispersoid fraction profiles

The homogenization simulation results were compared with measurements made using the EPMA shown in Table 2. The good agreement provides some confidence for the validity of the long-range diffusion sub-model. Another way to validate the simulation results is measuring the evolution of electrical resistivity, which is directly related to the solid solution solute level according to Matthiessen's law. For this AA3003 alloy, the formula suggested by Lok [10] is adopted:

$$\rho = 26.4 \text{ n}\Omega \cdot \text{m} + 31.1 \text{ n}\Omega \cdot \text{m} \cdot W_{\text{Mn}} \% + 19.7 \text{ n}\Omega \cdot \text{m} \cdot W_{\text{Fe}} \% + 6.2 \text{ n}\Omega \cdot \text{m} \cdot W_{\text{Si}} \% \quad (1)$$

Fig.3 shows the evolution of the calculated and measured resistivity for the whole homogenization process. They are in very good agreement until a local minimum is reached at around 500 °C. The resistivity increase after 500 °C is due to the swift response of the solubility in the primary phase to the temperature increase, which occurred due to the quick dissolution kinetics of the dispersoids at such a high temperature. Although both the simulation and the measurement show a peak resistivity following the local minimum, the simulated peak is reached earlier with a slightly higher value (51.6 nΩ·m vs 50.9 nΩ·m) than the measurement. The decrease of resistivity (so the solid solution solute level in the simulation) during the 600 °C soaking is due to the long range diffusion, which transported the solutes to the interdendritic constituent particles as evident in the compositional and dispersoid profiles shown in Fig. 1 and 2.

However, the simulated resistivity curve, which only accounted for solute effect, decreases much faster and to a much lower value (43.5 nΩ·m vs 47.5 nΩ·m) than the measured one. Among the many factors that might contribute to this discrepancy is the contribution of constituent particles to the resistivity in a fashion similar to insulators dispersed in a conducting phase. Lok [10] has discussed this composite effect for an AA3103 alloy and shown that the contribution from constitute particles could be described by  $\rho_{ppt} = \rho_{matrix} \left( (1 - f^{vol})^{-\frac{3}{2}} - 1 \right)$ . In our simulation, this composite effect had a peak contribution of 2.6 nΩ·m, half of which (1.3 nΩ·m) arose during the soaking. The curve with the

triangle marker in Fig. 3 shows the resistivity evolution curve accounting for both the solute and the composite effect.

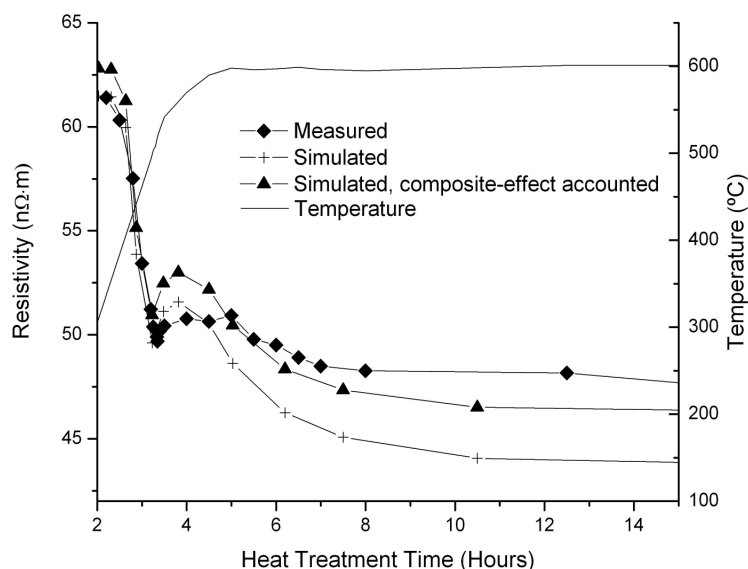


Fig.3 Evolutions of the calculated and measured resistivity during the heat treatment

## Conclusions

A fully CALPHAD-coupled model that is able to model microsegregation, nucleation, precipitation kinetics and long-range diffusion has been briefly introduced and applied to simulate the microstructural evolution during the solidification and homogenization heat treatment of an AA3003 alloy. The simulation results are in good agreement with EMPA and the electrical resistivity measurements indicating its predictive power and potential usages. The model output can readily be used as an input for downstream process models.

## Acknowledgement

The financial support from Rio Tinto Alcan and NSERC are gracefully acknowledged.

## References

- [1] Y.J. Li, L. Arnberg: *Acta Materialia* 51 (2003) 3415-3428.
- [2] Y.J. Li, L. Arnberg: *Materials Science and Engineering A347* (2003) 130-135.
- [3] Gandin Ch.-A, Jacot A: *Acta Materialia* 55 (2007) 2539-2553.
- [4] Z.J. Lok et al: *Materials Science Forum Vols. 519-521* (2006) 443-448.
- [5] Y.J. Li et al: *Materials Science Forum Vols. 519-521* (2006) pp 297-302.
- [6] M. Perez, M. Dumont, D. Acevedo-Reyes: *Acta Materialia* 56 (2008) 2119-2132.
- [7] Kenneth C. Russell: "Nucleation in Solids", presented at the American Society for Metals, 1968.
- [8] A. Jacot, M. Rappaz: *Acta Materialia* 50 (2002) 1909-1926.
- [9] Q. Du, A. Jacot: *Acta Materialia* 53 (2005) 3479-3493.
- [10] Z.J. Lok: Ph.D thesis, Delft University of Technology, 2005.